

## SIMULATION OF NON-FOURIER HEAT CONDUCTION IN DISCONTINUOUS HETEROGENEOUS MATERIALS BASED ON THE PERIDYNAMIC METHOD

by

**Luming ZHOU<sup>a,b</sup>, Zhende ZHU<sup>a,b</sup>, and Xiangcheng QUE<sup>a,b\*</sup>**

<sup>a</sup> Key Laboratory of Ministry of Education for Geomechanics and Embankment Engineering, Hohai University, Nanjing, China

<sup>b</sup> Jiangsu Research Center for Geotechnical Engineering Technology, Hohai University, Nanjing, China

Original scientific paper  
<https://doi.org/10.2298/TSCI220803157Z>

*Discontinuous heterogeneous materials, such as rocks and concrete, exhibit non-Fourier heat conduction. To predict this type of conduction behavior in discontinuous materials, a bond-based peridynamic heat conduction model based on the peridynamic theory was derived by introducing the dual-phase-lag model. The model was verified by the results obtained using other numerical methods. The Weibull distribution function was introduced to describe the heterogeneity in the thermal conductivity. The heat conduction in a plate with two pre-existing cracks under thermal shock was simulated. The effects of phase lag and heterogeneity were discussed. The results showed that the heat transfer rate is mainly controlled by the phase lag  $\tau_q$  of the heat flux. When  $\tau_q$  remains unchanged, the heat transfer rate increases with the increase in the phase lag  $\tau_T$  of the temperature gradient. The influence of cracks on the temperature field is mainly reflected in the area near the crack end. Although the temperature in the local area may be positively correlated with  $\tau_T$  in the short term, the long-term influence of the factor becomes increasingly weaker. The proposed method has a wide application prospect in simulating non-Fourier's heat conduction in discontinuous heterogeneous materials.*

*Key words: discontinuous heterogeneous material, peridynamics, phase lag, heat conduction, heterogeneity, non-Fourier's law*

### Introduction

Discontinuous heterogeneous materials, such as rocks and concrete, are widely found in nature and practical engineering [1, 2]. These materials often have discontinuities due to natural defects such as cracks. Heterogeneity refers to the change in the physical properties at each point in a specific physical field with the change in the spatial co-ordinates, such as the thermal conductivity in the temperature field and the permeability in the seepage field. Compared with continuous homogeneous materials, the heat conduction and temperature distribution in discontinuous heterogeneous materials are more complex. Studying the transient heat conduction in discontinuous heterogeneous materials is of great significance for engineering problems in various fields, such as in the exploitation of clean energy, including geothermal energy and shale gas from deep rock masses [3], thermomechanical coupling in nuclear reactors [4], and heat transfer in biological systems (such as tissues) [5].

\* Corresponding author, e-mail: 190204030004@hhu.edu.cn

Although Fourier's law has been proven to be suitable for simulating heat conduction problems in most engineering [6, 7], the heat wave is propagated with infinite rate. In practice, for some unsteady heat conduction processes under extreme heat transfer conditions, such as low and ultra-high temperatures, and heat transfer processes under micro-spatial scale conditions, the temperature changes suddenly, making Fourier's law inapplicable [8]. To overcome the limitations of Fourier's law in such cases, several new heat conduction models have been proposed. Here, two commonly used models are briefly introduced. Cattaneo [9] and Vernotte [10] proposed a hyperbolic heat conduction equation based on the existence of the relaxation time between the heat flow and the temperature gradient, namely the Cattaneo-Vernotte (CV) model. This model, however, only considers the case where the heat flow density lags behind the temperature gradient and does not conform to the Galilean invariant principle. Tzou [11] proposed a dual-phase-lag (DPL) model considering the phase lags of both the heat flux and temperature gradient. This model has been proven to be more effective and has been widely used in simulating the heat conduction in materials [12].

A non-Fourier's law heat conduction problem can be mainly solved using two types of methods: analytical methods and numerical methods. The former includes the Fourier transform method [13], variable separation method [14], integral transform method [15], and eigenvalue method [16]. The latter mainly includes the finite difference method [17], finite element method (FEM) [18], finite volume method (FVM) [19], extended finite element method (XFEM) [20], boundary element method (BEM) [21], and numerical manifold method (NMM) [22]. Compared with analytical methods, numerical methods have a wider application range and are more efficient. However, for discontinuous materials containing cracks, the element boundary in conventional numerical methods, such as the FEM, XFEM, and FVM, must be consistent with the boundary of the solution domain when meshing, and re-meshing must be done if the crack length changes. Because of its strong grid dependence, it is inconvenient to solve problems involving discontinuities and their evolution [23]. The BEM has the problem of singularity of variables when simulating discontinuous boundary. In NMM simulation, the crack can only extend to the edge of the element and cannot reach its interior.

Silling *et al.* [24-26] proposed the peridynamics (PD) theory and the corresponding numerical method. Unlike the classical heat conduction *local* theory, such as the FEM, which assumes that the heat flux density at a point is only determined by the temperature gradient at that point, the PD is a *non-local* theory, which discretizes a solid into a series of material points containing all the physical property information in the spatial domain. The heat flux density at each point is assumed to be affected by all the other points in the region of finite radius. In the process of heat conduction, the heat carrier carries heat from one material point to another. This process is essentially non-local, therefore, a non-local model can better describe the heat conduction phenomenon [27, 28]. In addition, unlike the classical continuum theory based on the derivative of the displacement component, the PD is based on the integral equation and overcomes the grid dependence when dealing with discontinuous problems.

The PD model has three forms: the bond-based (BB-PD), ordinary state-based (OSB-PD), and non-ordinary state-based models, among which the BB-PD model is the most widely used. In addition, BB-PD theory has fewer parameters and its constitutive model is easier to understand than the other two theories. Therefore, it is most convenient to use this theory to simulate the heat conduction of materials. In the application of BB-PD model in heat transfer problem, Gerstle *et al.* [29] proposed a PD framework that can simultaneously simulate the heat transfer, deformation, and electrical potential distribution in a 1-D electromigration process. Bo-baru and Duangpanya [30] studied 2-D heat conduction in discontinuous materials containing

cracks and in fiber-reinforced composites. Jafari *et al.* [31] studied the effect of using different kernel functions on PD heat conduction simulation results. In the application of OSB-PD model, Oterkus *et al.* [28] deduced a heat conduction formula for the OSB-PD model, this formula was later improved by Chen *et al.* [32], and its effectiveness was verified by comparing with the results obtained by Bobaru and Duangpanya [30]. Agwai *et al.* [33] deduced a fully coupled PD thermo-mechanical model and proposed a surface correction factor to improve the numerical simulation results. Liao *et al.* [34] proposed an improved OSB-PD model to simulate the transient heat conduction in functionally graded materials with thermally insulated cracks. Wang *et al.* [35] derived a OSB-PD heat conduction model based on the non-Fourier's law and verified that it can simulate heat conduction problems from the nanoscale to the macroscopic scale. Thus far, most PD simulations have been based on Fourier's law and adopt the macro equivalent thermal conductivity. The influence of discontinuity and heterogeneity on non-Fourier heat conduction is rarely considered.

In this study, the DPL model was introduced to derive a heat conduction model within the BB-PD theoretical framework based on the non-Fourier's law, and a PD numerical implementation method for a discontinuous material containing cracks under thermal boundary conditions was introduced. The feasibility of the model was verified by three numerical examples. The Weibull distribution function was introduced to reflect the heterogeneity in the thermal conductivity of the materials, and the heat conduction behavior of a plate with pre-existing cracks under thermal shock was simulated. The effects of phase lag of the heat flux, phase lag of the temperature gradient and heterogeneity on the distribution law of the temperature field and heat transfer rate were investigated. It is expected that this study could provide theoretical reference for engineering problems such as geothermal energy or shale gas exploitation, so as to improve the corresponding resource exploitation efficiency.

## Theory and methods

### The PD for heat conduction based on Fourier's law

Unlike the classical local theory, which only considers the interaction between points in contact with material points, the PD theory, as a non-local theory, assumes that at any time,  $t$ , any point  $\mathbf{x}$  in the object has an interaction  $f_T(\mathbf{x}', \mathbf{x}, t)$  with any other point  $\mathbf{x}'$  in a certain area  $H_x$  around it. The  $H_x$  is the horizon of  $\mathbf{x}$ . The concept of horizon can be expressed:

$$H_x = H(\mathbf{x}, \delta) = \{\mathbf{x} \in R : |\mathbf{x}' - \mathbf{x}| \leq \delta\} \quad (1)$$

where  $\delta$  is the radius of  $H_x$ .

In problems based on Fourier's law, it is assumed that the heat flux  $f_T$  between points  $\mathbf{x}$  and  $\mathbf{x}'$  is a function of only the temperature difference between these two points, and the heat conduction equations for the BB-PD model are:

$$\mathbf{q}(\mathbf{x}, t) = -k_T \nabla T(\mathbf{x}, t) \quad (2)$$

$$\rho c \frac{\partial T(\mathbf{x}, t)}{\partial t} = \int_{H_x} f_T(T', T, \mathbf{x}', \mathbf{x}, t) dV_{x'} + S_b(\mathbf{x}, t) \quad (3)$$

$$Q(\mathbf{x}, t) = \int_{H_x} f_T(T', T, \mathbf{x}', \mathbf{x}, t) dV_{x'} \quad (4)$$

where  $\mathbf{q}$  is the heat flux vector,  $k_T$  – the thermal conductivity,  $\nabla T$  – the temperature gradient,  $\rho$  and  $c$  are the density and specific heat capacity, respectively,  $dV_{x'}$  – the infinitesimal volume linked to point  $x'$ ,  $S_b$  – the heat generated by the heat source per unit time and unit volume, and  $Q$  – the heat flow.

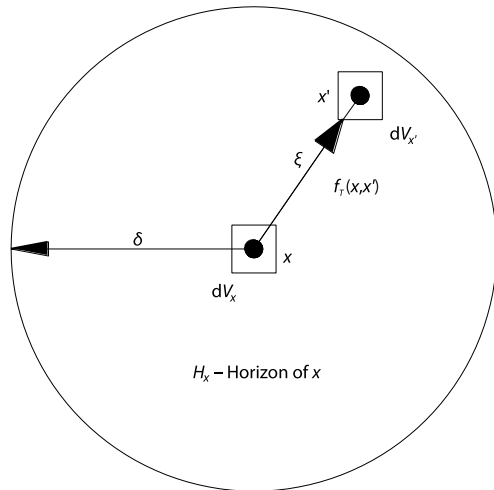


Figure 1. Schematic of PD for heat conduction

As shown in fig. 1, points  $x$  and  $x'$  interact through a *thermal bond*. The  $\xi$  represents their relative position vector:

$$\xi = \mathbf{x}' - \mathbf{x} \quad (5)$$

The heat flux  $f_T$  between points  $x$  and  $x'$  can be expressed [27]:

$$f_T(T', T, \mathbf{x}', \mathbf{x}, t) = \kappa_T \frac{\tau(\mathbf{x}', \mathbf{x}, t)}{|\xi|} \quad (6)$$

$$\tau(\mathbf{x}', \mathbf{x}, t) = T'(\mathbf{x}', t) - T(\mathbf{x}, t) \quad (7)$$

where  $\kappa_T$  is the micro thermal conductivity. Based on the temperature field with a linear change, Oterkus *et al.* [28] derived expressions for the micro thermal conductivity in 2-D space through an equivalent analysis of the PD thermal potential and classical thermal potential at certain points:

$$\kappa_T = \frac{6k_T}{\pi h \delta^3} \quad (8)$$

#### The PD for heat conduction based on non-Fourier's law

The DPL model proposed by Tzou [11] is introduced into the theoretical framework of the BB-PD heat conduction model:

$$q(\mathbf{x}, t + \tau_q) = -k_T \nabla T(\mathbf{x}, t + \tau_T), \quad \tau_q > 0, \quad \tau_T > 0 \quad (9)$$

Equation (4) can be re-written:

$$Q(\mathbf{x}, t + \tau_q) = \int_{H_x} f_T(T', T, \mathbf{x}', \mathbf{x}, t + \tau_T) dV_{x'} \quad (10)$$

where  $\tau_T$  and  $\tau_q$  are the phase lags of the temperature gradient and heat flux vector, respectively. When  $\tau_T = 0$ , the DPL model degenerates into a wave model [35]. When  $\tau_T = \tau_q = 0$ , it degenerates into a Fourier heat conduction model.

The non-Fourier heat conduction model of the BB-PD can be obtained by the first-order Taylor expansion of the function terms concerning  $t$  on the left- and right-hand sides of eq. (10):

$$\begin{aligned} \rho c \frac{\partial T(\mathbf{x}, t)}{\partial t} + \tau_q \rho c \frac{\partial^2 T(\mathbf{x}, t)}{\partial t^2} &= \int_{H_x} f_T(T', T, \mathbf{x}', \mathbf{x}, t) dV_{x'} + \\ &+ \tau_T \int_{H_x} \frac{\partial f_T(T', T, \mathbf{x}', \mathbf{x}, t)}{\partial t} dV_{x'} + S_b(\mathbf{x}, t) + \tau_q \frac{\partial S_b(\mathbf{x}, t)}{\partial t} \end{aligned} \quad (11)$$

### Numerical implementation

#### Discretization

A quadrature method was adopted to solve eq. (11). As shown in fig. 2, the entire model is uniformly dispersed into multiple subdomains, and the temperature at each subdomain is considered a constant. Heat flows from the geometric center point of the high temperature subdomain to the geometric center point of the low temperature subdomain, and the distance between any two center points is  $\Delta x$ . At a certain time,  $t$ , the volume integration in eq. (11) can be replaced:

$$\rho_i c_i \frac{\partial T_i(\mathbf{x}, t)}{\partial t} + \tau_{qi} \rho_i c_i \frac{\partial^2 T_i(\mathbf{x}, t)}{\partial t^2} = \sum_{j=1}^N \left[ f_{Tij}(\mathbf{x}', \mathbf{x}, t) + \tau_T \frac{\partial f_{Tij}(\mathbf{x}', \mathbf{x}, t)}{\partial t} \right] V_j + S_{bi}(\mathbf{x}, t) + \tau_{qi} \frac{\partial S_{bi}(\mathbf{x}, t)}{\partial t} \quad (12)$$

where  $i$  is the material point of interest,  $N$  – the total number of subdomains within the horizon of point  $i$ , and  $V_j$  – the volume of the subdomain at point  $\mathbf{x}_j$ .

For the material points on the horizon boundary, the node volume should be corrected [27]:

$$V_j = \begin{cases} (\Delta x)^3, & |\xi| \leq (\delta - d) \\ \left( \frac{\delta + d - \|\xi\|}{2d} \right) (\Delta x)^3, & (\delta - d) < |\xi| \leq \delta \\ 0, & |\xi| > \delta \end{cases} \quad (13)$$

where  $d$  is half of  $\Delta x$ .

Equation (12) is solved using the explicit central-difference time integration technique:

$$\frac{\partial T_i^{n+1}}{\partial t} = \frac{\partial^2 T_i^n}{\partial t^2} \Delta t + \frac{\partial T_i^n}{\partial t} \quad (14)$$

$$T_i^{n+1} = \frac{\partial T_i^{n+1}}{\partial t} \Delta t + T_i^n \quad (15)$$

where  $n$  is the number of time steps and  $\Delta t$  – the time step. According to Wang *et al.* [35],  $\Delta t$  should satisfy:

$$\Delta t < \frac{\rho_i c_i}{P_0} \left[ \sqrt{\left( 1 + \frac{P_0 \tau_T}{\rho_i c_i} \right)^2 + \frac{4P_0 \tau_q}{\rho_i c_i}} - \left( 1 + \frac{P_0 \tau_T}{\rho_i c_i} \right) \right], \quad P_0 = \sum_{j=1}^N \frac{2\kappa}{|\xi|} V_j \quad (16)$$

#### Boundary conditions

The boundary conditions in a PD heat conduction problem can be the temperature, heat flux, radiation, and conduction. As shown in fig. 3, the region of the studied material

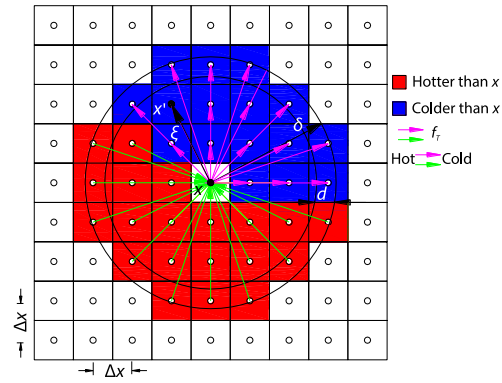


Figure 2. Diagrammatic sketch of discretization

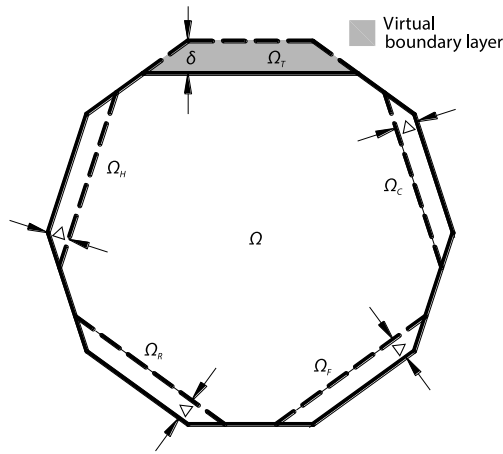


Figure 3. Boundary-layer with the temperature, heat flux, radiation, and convection

is  $\Omega$ , and the temperature boundary condition should be applied to the virtual boundary-layer  $\Omega_r$ , which is outside the real surface of the material, and its depth is equal to the size of the PD region  $\delta$  [27]. The other three temperature boundary conditions can be directly applied to the boundary within the real material area  $\Omega$ , that is,  $\Omega_H$ ,  $\Omega_R$ , and  $\Omega_C$  in fig. 3, and the depth is the discrete spacing  $\Delta x$ .

In this study, the boundary conditions of only the temperature and heat flux were considered:

$$T_i = T_{bt}, \quad i \in \Omega_r \quad (17)$$

$$q_i = q_{bt}, \quad i \in \Omega_H \quad (18)$$

where  $i$  represents the  $i^{\text{th}}$  material point,  $T_{bt}$  – the boundary temperature, and  $q_{bt}$  – the heat flux at the boundary.

If no condition is applied at the boundary, that is, when the boundary is free, the heat flux in the boundary-layer region  $\Omega_F$  is 0:

$$q_i^{n'} = 0, \quad i \in \Omega_F \quad (19)$$

where  $n'$  is the normal vector to the boundary surface.

**Model validation**

To verify that the PD model established in this study can effectively simulate the heat conduction in continuous and discontinuous materials, the heat transfer in a homogeneous square plate (containing pre-existing cracks) subjected to thermal shock load was simulated. The results were compared with those obtained by Tehrani *et al.* [36] and Madenci and Oterkus [27] using other numerical methods. Figure 4 shows the geometric model of a homogeneous square plate. Table 1 shows the numerical parameters.

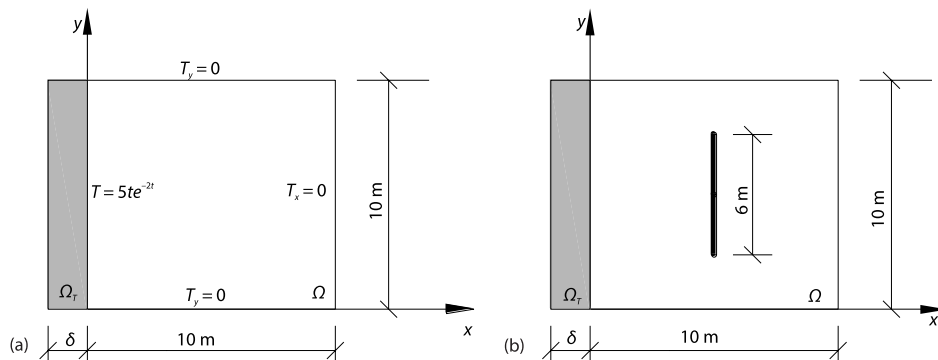


Figure 4. Geometric model of a 2-D homogeneous square plate; (a) without pre-existing crack and (b) with pre-existing crack

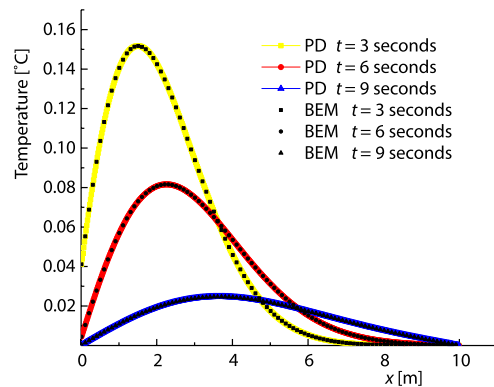
**Table 1. Parameters of a 2-D homogeneous square plate model**

Parameter	Value	Parameter	Value
Length × width ( $L \times D$ )	10 m × 10 m	Density, $\rho$	1 kg/m <sup>3</sup>
Thickness, $H$	0.02 m	Number of points in $x$ - and $y$ - directions	500 × 500
Crack length, $H_f$	6 m	Point spacing, $\Delta$	0.02 m
Specific heat capacity, $c$	1 J/kg/K	Radius of horizon, $\delta$	3.015 $\Delta$
Thermal conductivity, $k_T$	1 W/m/K	Time step, $\Delta t$	0.0005 second

The initial and boundary conditions are:

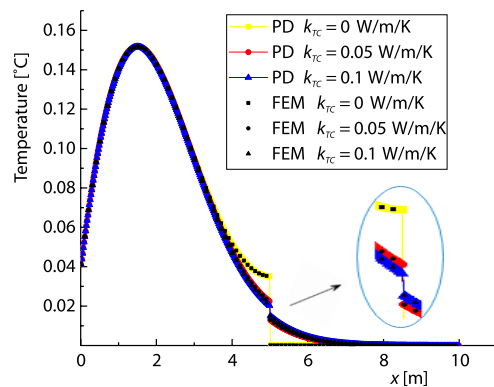
$$\begin{aligned}
 T(x, y, t = 0) &= 0 \\
 T(x = 0, t) &= 5te^{-2t}, \quad \frac{\partial T}{\partial x}(x = 10, y) = 0, \quad t > 0 \\
 \frac{\partial T}{\partial y}(x, y = \pm 5) &= 0, \quad t > 0
 \end{aligned}
 \tag{20}$$

Figure 5 shows the results of the temperature distribution on the square plate at  $y = 5$  m without any pre-existing crack at  $t = 3$  seconds,  $t = 6$  seconds and  $t = 9$  seconds, as measured using the PD and BEM [36]. The wave propagates from left to right and gradually widens as it propagates. The temperature first increases and then decreases along the  $x$ -axis direction. The peak temperature decreases gradually as the wave propagates, however, it decreases more gradually along the  $x$ -axis. The prediction results of the PD and BEM are consistent.



**Figure 5. Temperature distribution at  $y = 5$  m on a square plate without pre-existing crack, obtained using the PD and BEM [36]**

Figure 6 shows the results of the temperature distribution at  $y = 5$  m on a square plate with a pre-existing crack, obtained using the PD and FEM [27] under different crack thermal conductivity values with 0, 0.05, and 0.1 W/m/K. Compared with the square plate without any crack, the slope of the temperature curve at the discontinuity ( $x = 5$  m) is greater, that is, the temperature gradient at the crack is higher. The temperature gradient decreases with the increase in  $k_{TC}$ , however, the decreasing rate reduces. The simulation results of the PD, BEM, and FEM are consistent, demonstrating that the PD model employed in this study can effectively simulate the heat conduction in continuous and discontinuous materials.



**Figure 6. Temperature distribution on a plate with a pre-existing crack at  $y = 5$  m**

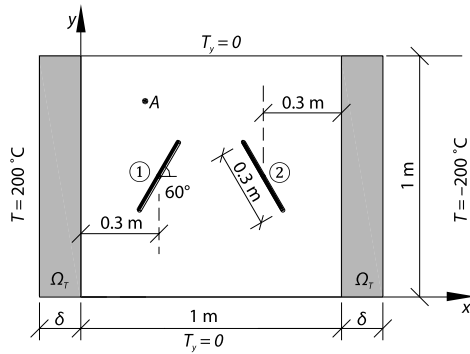


**Figure 7. Geometric model of a rock plate with adiabatic cracks**

The rock plate is discretized into  $100 \times 100$  material points, node spacing  $\Delta x = 0.01$  m, time step  $\Delta t = 1 \times 10^{-6}$  seconds, and the other parameters are the same as those listed in tab. 1.

#### Effect of phase lags

Given the lack of reliable experimental value of the thermal relaxation time for rocks [37, 38], four representative phase lag values (2, 0.2, 0.02, and 0.002 seconds) were selected to cover different states of the heat conduction behavior.

Figure 8 shows the temperature field distribution of the plate at 0.1 second under different  $\tau_q$  and  $\tau_T$  values. Each row represents a different  $\tau_q$  value, and each column represents a different  $\tau_T$  value. By comparing the diagrams of different columns in the same row, it can be found that when the phase lag  $\tau_T$  of the temperature gradient decreases from 2 seconds to 0.002 seconds, the heat transfer rate gradually decreases. This phenomenon is evident when the phase lag  $\tau_q$  of the heat flux is 2 seconds or 0.2 seconds, whereas when  $\tau_q$  is 0.02 seconds or 0.002 seconds, the effect of  $\tau_T$  on the heat transfer rate cannot be observed directly from the diagram.

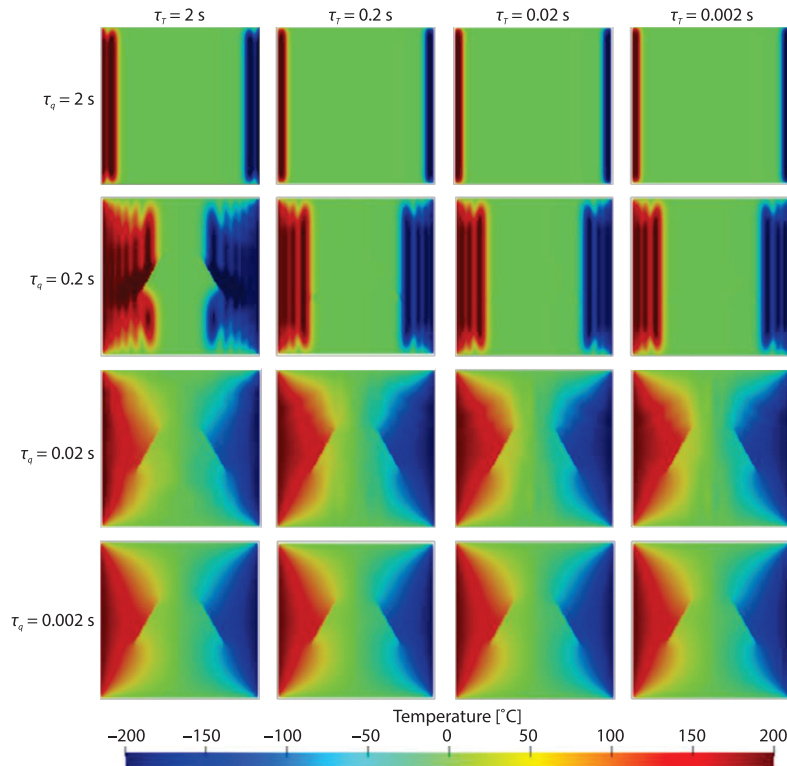
When  $\tau_q$  is 2 second, the heat transfer rate is low and the effect of crack is not reflected. When  $\tau_q$  is 0.02 second or 0.002 second, or when  $\tau_q$  is 0.2 second and  $\tau_T$  is 1 second, it can be seen that the high/low temperature region is distributed along the crack, the isotherm is concentrated near the crack tip, and the discontinuity of heat conduction is significant, which is similar to the result obtained by Wang *et al.* [35].

Figure 9 shows the temperature field distribution at 0.1 second when  $\tau_T = 0$ . Combined with figs. 8 and 9, it can be found that  $\tau_q$  plays a major role in the heat transfer. The lower the  $\tau_q$  value, the faster the heat transfer. When  $\tau_q$  decreases to a certain value (0.2 second), the distribution law of the temperature field is related to the relative magnitudes of  $\tau_T$  and  $\tau_q$ . When  $\tau_T > \tau_q$ , the temperature distribution is dominated by  $\tau_q$ , the heat propagation speed is high, and the temperature field shows evident discontinuous characteristics. When  $\tau_T \leq \tau_q$ , the heat conduction speed is low, and the influence of crack on the heat conduction is not reflected.

To more specifically study the influence of  $\tau_q$  and  $\tau_T$  on the heat conduction, fig. 10 shows the temperature curve at measuring Point A (0.25, 0.75) with respect to time. In fig. 10(a), as  $\tau_q (= 1$  second) is significantly greater than 0.1 second, the temperature increases only when  $\tau_T = \tau_q$ , and the increase is in a narrow range of  $5.4 \times 10^{-6}$  °C. The relative trend in the temperature curves under different  $\tau_T$  values also appears when  $\tau_q$  is 0.2 second, fig. 10(b). The difference is that when  $\tau_T = 1$  second, thermal diffusion is evident, and the temperature reaches 200 °C at 0.086 second, whereas in other cases where  $\tau_T \leq \tau_q$ , the heat transfer rate is relatively low. In fig.

#### Heat conduction in a plate with adiabatic cracks

As shown in fig. 7, the dimensions of the rock plate are  $1 \text{ m} \times 1 \text{ m}$ . The plate contains two adiabatic cracks ① and ②, each with a length of 0.3 m and located 0.3 m away from the left and right boundaries of the plate. The included angle between crack ① and the positive direction of the x-axis is  $60^\circ$ , and the two cracks are symmetrically distributed. The initial temperature is  $0 \text{ }^\circ\text{C}$ , the left and right boundaries are subjected to thermal shock with magnitudes of  $200 \text{ }^\circ\text{C}$  and  $-200 \text{ }^\circ\text{C}$ , respectively, and the heat flux density of the upper and lower boundaries is 0. The rock



**Figure 8. Temperature field distribution at 0.1 second under different  $\tau_q$  and  $\tau_T$  values**

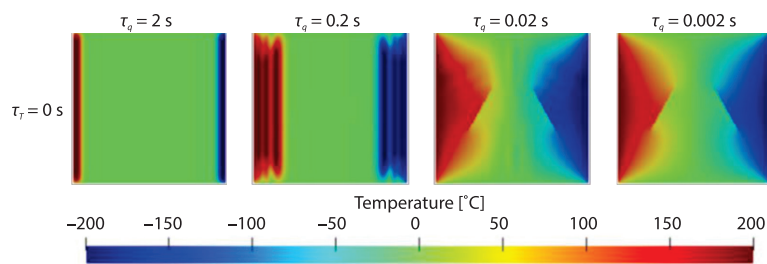


**Figure 9. Temperature field distribution at 0.1 second when  $\tau_T = 0$**

10(c), when  $\tau_q = 0.02$  seconds, the fluctuation characteristics of heat conduction are evident, and the greater the  $\tau_T$  value, the faster the heat transfer, the higher the temperature peak, and the wider the fluctuation range, consistent with the results obtained by Narasimhan and Sadasivam [5]. In fig. 10(d), when  $\tau_q = 0.002$  seconds, the heat propagation mode tends to follow the Fourier's heat conduction law, fig. 10(e), and the lower the  $\tau_T$  value, the closer it is.

A general rule is evident in figs. 10(a)-10(d), with the increase in  $\tau_T$ , the higher the phase lag of the temperature gradient, the higher the temperature at Point A at the same point in time. However, fig. 10(d) shows that the long-term response is the same under different  $\tau_T$  conditions, and it finally tends to the steady-state of the same value. (When  $\tau_q = 2$  seconds, 0.2 seconds, 0.002 seconds, 0.0002 seconds, and 0 seconds, the corresponding final constant temperature is 79.0 °C, 78.3 °C, 77.3 °C, 77.2 °C, and 77.1 °C.)

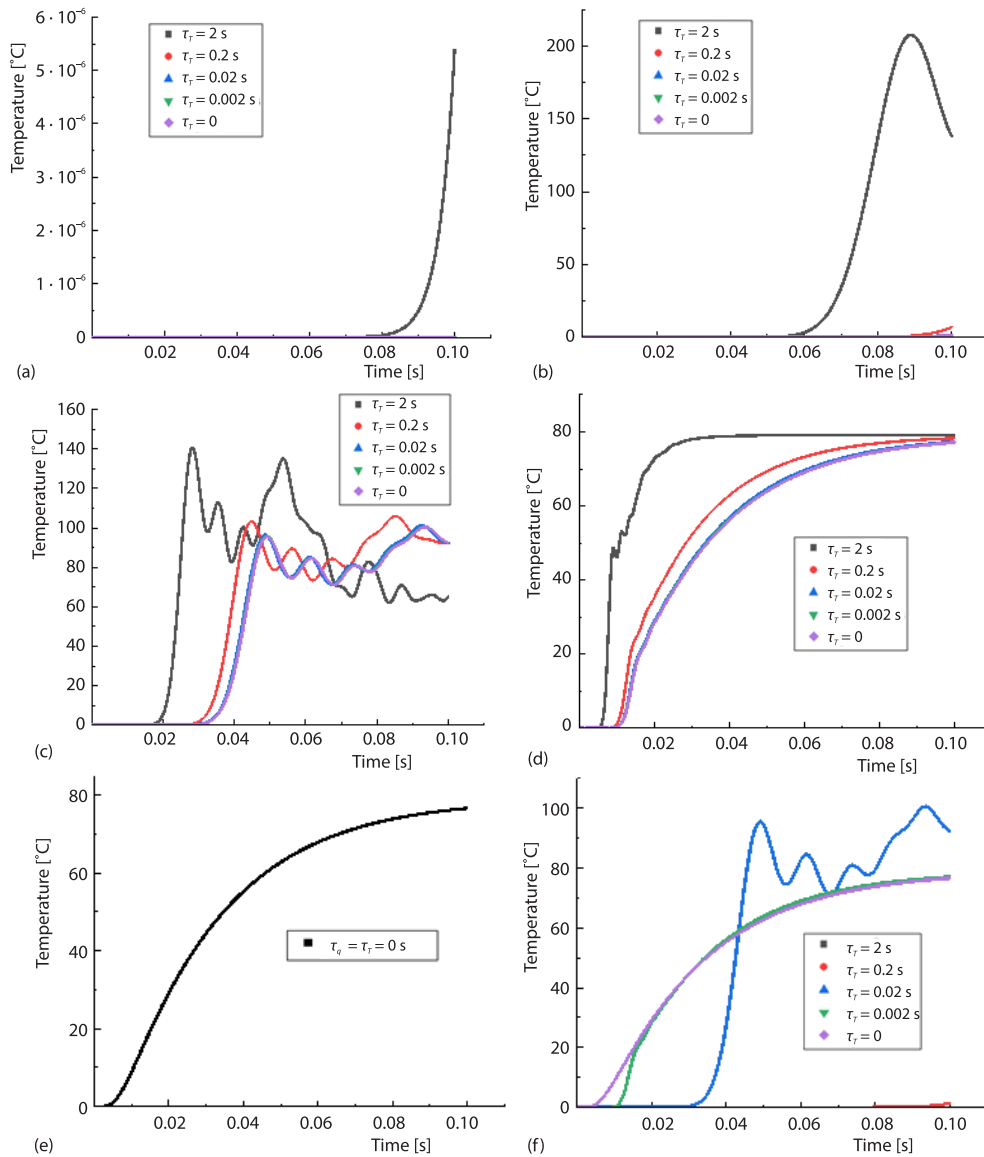


**Figure 10.** Temperature change curve at Point A under different  $\tau_q$  and  $\tau_T$  values; (a)  $\tau_q = 2$  s, (b)  $\tau_q = 0.2$  s, (c)  $\tau_q = 0.02$  s, (d)  $\tau_q = 0.002$  s, (e)  $\tau_q = \tau_T = 0$ , and (f)  $\tau_T = 0$

When  $\tau_T = 0$ , fig. 10(f), the DPL model degenerates into a hyperbolic heat conduction model. When  $\tau_q$  is 2 second or 0.2 second, the heat transfer rate is low, and the temperature change at Point A is small. When  $\tau_q = 0.02$  seconds, the temperature at Point A rises first and then fluctuates. When  $\tau_q$  is 0.002 second or 0 second, the temperature at Point A changes in the form of a parabola, and when  $\tau_q = 0.002$  seconds, the temperature in the initial stage is slightly lower than that when  $\tau_q = 0$  seconds. This is because the delay in the heat flux decreases the rate of heat diffusion. However, as time progresses, the influence of  $\tau_q$  becomes increasingly less, and the temperature curves of the two tend to coincide.

*Effect of the degree of homogeneity*

In practical engineering, many materials are heterogeneous, such as rocks and concrete. The heat conduction conditions at each point in these materials may be different. In previous studies, some researches have found that Weibull distribution can be used to describe the heterogeneity of rocks and concrete [39, 40]. Therefore, Weibull distribution is used to describe the heterogeneous characteristics of the thermal conductivity of materials in this study:

$$We(s) = \frac{r}{s_0} \left(\frac{s}{s_0}\right)^{r-1} \exp\left[-\left(\frac{s}{s_0}\right)^r\right] \tag{21}$$

where  $s$  is the distribution parameter value satisfied by each point,  $s_0$  – the average value of the parameter  $s$ , and  $r$  – the homogeneity of the material structure.

Assuming that the thermal conductivity,  $k$ , at each point in the material obeys the Weibull distribution function with a mean value of 1, the heat conduction behavior when  $r = 2, 5, 10,$  and  $100$  was simulated. Figure 11 shows the probability density map of Weibull distribution function when  $k = 1$ . Figure 12 shows the thermal conductivity distribution on the plate with different  $r$  values. Combined with figs. 11 and 12, it can be seen that when scale parameter is a constant, the lower the  $m$  value, the more discrete the distribution of the thermal conductivity, the greater the  $m$  value, the closer the thermal conductivity is to the mean value.

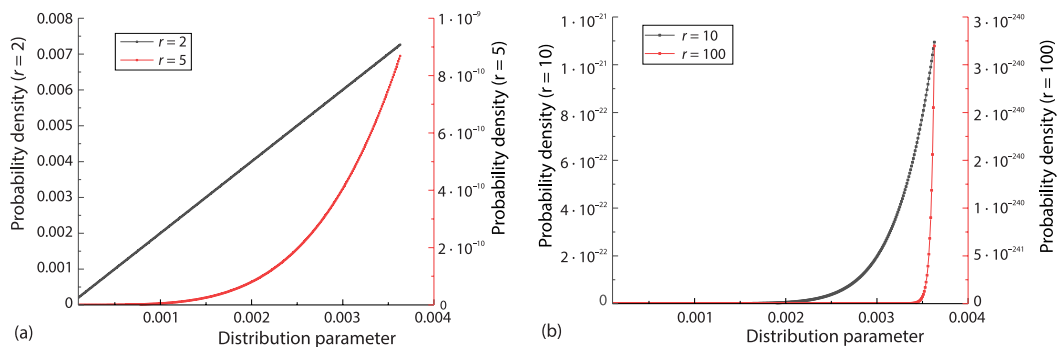


**Figure 11. Probability density map of Weibull distribution function; (a)  $r = 2$  and 5 and (b)  $r = 10$  and 100**

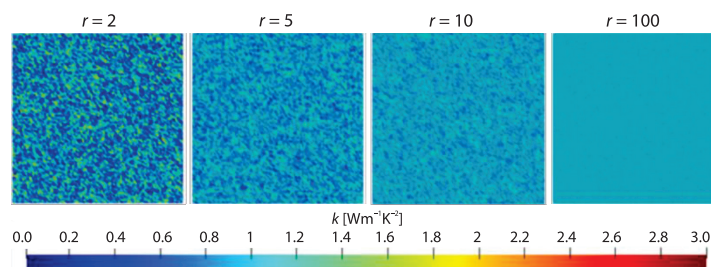


**Figure 12. Thermal conductivity distributions under different degrees of homogeneity**

It is assumed that  $\tau_q = 0.02$  seconds and  $\tau_T = 2$  seconds. Figure 13 shows the temperature field distribution at 0.1 second under different homogeneity conditions. When  $r = 2$ , the heterogeneity of the plate is the strongest, and the temperature field distribution is the most irregular. There are evident *abnormal values* in the left red high temperature (LRHT) region

and the right blue low temperature (RBLT) region due to the heterogeneity of the thermal conductivity. In other cases, the LRHT and RBLT regions remain symmetrically distributed.

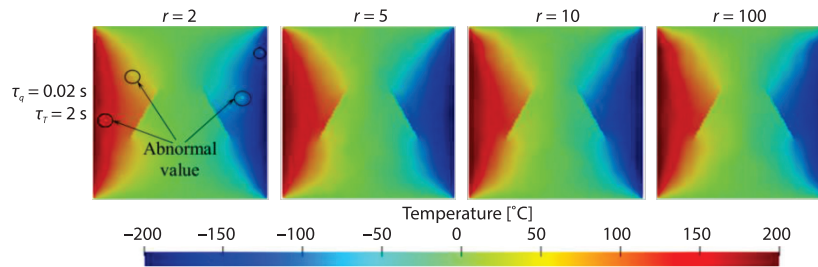


Figure 13. Temperature field distributions under different degrees of homogeneity

Figure 14 shows the temperature change curve at Point A with respect to time under different homogeneity conditions. Regardless of the  $\tau_q$  value, the temperature at the same point in time decreases with the enhancement in the heterogeneity. Moreover, fig. 13(a) shows that when  $r = 2, 5, 10,$  and  $100$ , the time of the first peak is  $0.038$  second,  $0.0303$  second,  $0.029$  second, and  $0.028$  second, respectively. That is, the stronger the heterogeneity, the later the appearance of the temperature peak. Figure 13(b) shows that the temperature values under various homogeneity conditions are the same after approximately  $0.07$  second. That is, the enhancement in the heterogeneity temporarily reduces the temperature value at Point A. However, under the action of relatively long-term heat conduction, the degree of homogeneity will not have a significant impact on the temperature value at Point A.

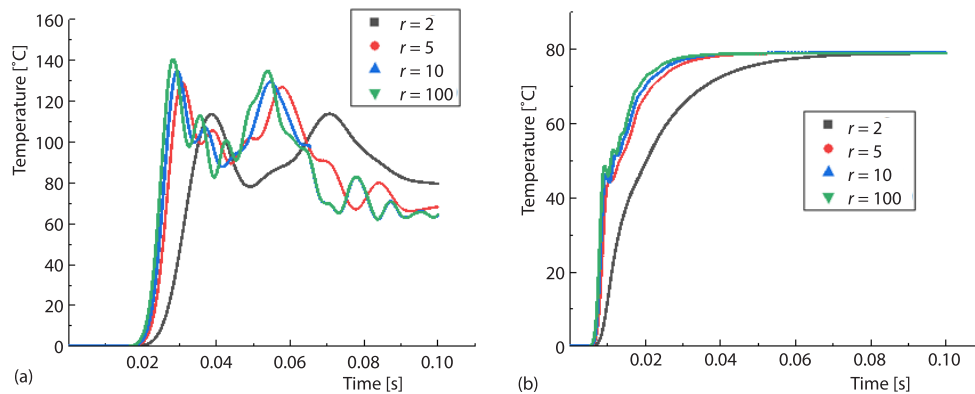


Figure 14. Temperature change curve at point A under different degrees of homogeneity; (a)  $\tau_q = 0.02$  s,  $\tau_T = 2$  s and (b)  $\tau_q = 0.002$  s,  $\tau_T = 2$  s

## Conclusions

In this work, a heat conduction model within the framework of the BB-PD theory was derived by introducing the DPL model. On this basis, the effects of phase lag and degree of homogeneity on the heat conduction behavior in discontinuous heterogeneous materials were studied. The main conclusions are as follows.

- The derived PD heat conduction model can effectively simulate the non-Fourier's heat conduction process in discontinuous materials; this was confirmed by comparing the simulation result of a homogeneous square plate with pre-existing cracks subjected to thermal shock load and the theoretical result of a 1-D model of a human tissue with blood perfusion.

- The phase lag  $\tau_q$  of the heat flux plays a major role in the heat transfer. When  $\tau_q$  is constant, the heat transfer rate increases with the increase in the phase lag  $\tau_T$  of the temperature gradient.
- The distribution law of the thermal conductivity based on the Weibull function can well reflect the heterogeneity of materials. For a specific point, the heat transfer rate may increase with the increase in the heterogeneity in a short duration.
- The distribution shape of the temperature field is dominated by crack characteristics, and the influence of cracks on the temperature field distribution is mainly reflected in the area near the crack end. For the temperature at a specific point, although  $\tau_T$  may have a positive correlation in the short term, and the heterogeneity may have a negative correlation, the influence of the aforementioned factors becomes increasingly weaker after a relatively long time.

### Acknowledgment

This work was funded by the Postgraduate Research and Practice Innovation Program of Jiangsu Province (KYCX22\_0613), National Natural Science Foundation of China (Grant Nos. 41831278, 51878249, and 51579081). The authors would like to thank all the reviewers who participated in the review and MJEditor ([www.mjeditor.com](http://www.mjeditor.com)) for its linguistic assistance during the preparation of this manuscript.

### Nomenclature

$c$  – specific heat capacity, [(Jkg<sup>-1</sup>)K<sup>-1</sup>]  
 $f_T$  – heat flux  
 $H_x$  – the horizon of point  $x$   
 $k_T$  – thermal conductivity  
 $n$  – the number of time steps  
 $Q$  – heat flow, [Wm<sup>-3</sup>]  
 $q$  – heat flux vector  
 $S_b$  – heat source, [Wm<sup>-3</sup>]  
 $T$  – temperature, [°C]  
 $t$  – time, [second]  
 $\Delta t$  – time step, [second]  
 $V$  – volume, [m<sup>3</sup>]

#### Greek symbols

$\delta$  – radius of the horizon, [mm]  
 $\kappa_T$  – micro thermal conductivity  
 $\rho$  – density, [kgm<sup>-3</sup>]

$\tau$  – temperature difference, [°C]  
 $\tau_q$  – phase lag of the heat flux vector, [second]  
 $\tau_T$  – phase lag of the temperature gradient, [second]

#### Acronyms

BB-PD – bond-based peridynamics  
BEM – boundary element method  
CV – Cattaneo-Vernotte  
DPL – dual-phase-lag  
FEM – finite element method  
FVM – finite volume method  
LRHT – left red high temperature  
NMM – numerical manifold method  
OSB-PD – ordinary state-based peridynamics  
PD – peridynamics  
RBLT – right blue low temperature  
XFEM – extended finite element method

### References

- [1] Wang, Y. T., Zhou, X. P., Peridynamic Simulation of Thermal Failure Behaviors in Rocks Subjected to Heating From Boreholes, *Int. J. Rock Mech. Min. Sci.*, 117 (2019), Mar., pp. 31-48
- [2] Jin, Y., *et al.*, Numerical Study of Shrinkage and Heating Induced Cracking in Concrete Materials and Influence of Inclusion Stiffness with Peridynamics Method, *Comput. Geotech.*, 133 (2021), Feb., 103998
- [3] Zhou, L., *et al.*, Coupled Thermal-Hydraulic-Mechanical Model for an Enhanced Geothermal System and Numerical Analysis of Its Heat Mining Performance, *Renew. Energy*, 181 (2022), Jan., pp. 1440-1458
- [4] Lee, C., *et al.*, Numerical Analysis of Coupled Thermo-Hydro-Mechanical Behavior in Single- and Multi-Layer Repository Concepts for High-Level Radioactive Waste Disposal, *Tunn. Undergr. Sp. Technol.*, 103 (2020), Sept., pp. 1-17
- [5] Narasimhan, A., Sadasivam, S., Non-Fourier Bio Heat Transfer Modelling of Thermal Damage during Retinal Laser Irradiation, *Int. J. Heat Mass Transf.*, 60 (2013), May, pp. 591-597
- [6] Dass, A., Gedupudi, S., Fourier Series Based 1-D Numerical Modelling of the Dynamics of Inclined Closed Loop Buoyancy Driven Heat Exchangers with Conjugate Effect, *Int. J. Therm. Sci.*, 167 (2021), 106987

- [7] Furmanski, P., Łapka, P., Micro-Macro Heat Conduction Model for the Prediction of Local, Transient Temperature In Composite Media, *Int. J. Therm. Sci.*, 154 (2020), 106401
- [8] Nawaz, M., et al., Thermal and Solutal Analysis in Power Law Fluid under Non-Fourier's Diffusion Conditions, *Int. Commun. Heat Mass Transf.*, 126 (2021), 105331
- [9] Cattaneo, C., A Form of Heat Conduction Equation Which Eliminates the Paradox of Instantaneous Propagation, *Compte Rendus*, 247 (1958), Jan., pp. 431-433
- [10] Vernotte, P., Paradoxes in the Continuous Theory of the Heat Conduction, *Compte Rendus*, 246 (1958), pp. 3154-3155
- [11] Tzou, D. Y., A Unified Field Approach for Heat Conduction From Macro- To Micro-Scales, *Journal Heat Transfer*, 117 (1995), 1, pp. 8-6
- [12] Bazzara, N., et al., Numerical Analysis of A Dual-Phase-Lag Model with Microtemperatures, *Appl. Numer. Math.*, 166 (2021), Aug., pp. 1-25
- [13] Hobiny, A. D., Abbas, I. A., A Dual-Phase-Lag Model of Photothermoelastic Waves in A 2-D Semiconducting Medium, *Phys. Mesomech.*, 23 (2020), 2, pp. 167-175
- [14] Ghasemi, M. H., et al., Numerical Analysis of Non-Fourier Heat Transfer in a Solid Cylinder with Dual-Phase-Lag Phenomenon, *C. - Comput. Model. Eng. Sci.*, 122 (2020), 1, pp. 399-414
- [15] Abouelregal, A. E., Two-Temperature Thermoelastic Model without Energy Dissipation Including Higher Order Time-Derivatives and Two-Phase-Lags, *Mater. Res. Express*, 6 (2019), 11
- [16] Othman, M. I. A., Abbas, I. A., Eigenvalue Approach for Generalized Thermoelastic Porous Medium under the Effect of Thermal Loading Due to a Laser Pulse in DPL Model, *Indian J. Phys.*, 93 (2019), 12, pp. 1567-1578
- [17] Akula, S. C., Maniyeri, R., Numerical Simulation of Bioheat Transfer: A Comparative Study on Hyperbolic and Parabolic Heat Conduction, *Journal Brazilian Soc. Mech. Sci. Eng.*, 42 (2020), 1, pp. 1-13
- [18] Upadhyay, S., Rai, K. N., A New Iterative Least Square Chebyshev Wavelet Galerkin FEM Applied to Dual Phase Lag Model on Microwave Drying of Foods, *Int. J. Therm. Sci.*, 139 (2019), May, pp. 217-231
- [19] Kheirandish, Z., et al., Numerical Study into the Fin Performance Subjected to Different Periodic Base Temperatures Employing Fourier and Non-Fourier Heat Conduction Models, *Int. Commun. Heat Mass Transf.*, 114 (2020), 104562
- [20] Rannou, J., et al., The 3-D Experimental and Numerical Multiscale Analysis of a Fatigue Crack, *Comput. Methods Appl. Mech. Eng.*, 199 (2010), 21-22, pp. 1307-1325
- [21] Supriyono, Abadi, M. H. A., Dual Boundary Element Method for Elastoplastic Fracture Mechanics of Shear Deformable Plate, *Eng. Anal. Bound. Elem.*, 117 (2020), Aug., pp. 132-142
- [22] Wu, Z., Wong, L. N. Y., Frictional Crack Initiation and Propagation Analysis Using the Numerical Manifold Method, *Comput. Geotech.*, 39 (2012), 1, pp. 38-53
- [23] Yang, Z., et al., Peridynamic Simulation of Fracture Mechanical Behaviour of Granite Specimen under Real-Time Temperature and Post-Temperature Treatments, *Int. J. Rock Mech. Min. Sci.*, 138 (2021), Dec., 104573
- [24] Silling, S. A., Reformulation of Elasticity Theory for Discontinuities and Long-Range Forces, *Journal Mech. Phys. Solids*, 48 (2000), 1, pp. 175-209
- [25] Silling, S. A., Askari, E., A Meshfree Method Based on the Peridynamic Model of Solid Mechanics, *Computers and Structures*, 83 (2005), 17-18, pp. 1526-1535
- [26] Silling, S. A., et al., Peridynamic States and Constitutive Modelling, *Journal Elast.*, 88 (2007), 2, pp. 151-184
- [27] Madenci, E., Oterkus, E., *Peridynamic Theory and Its Applications*, Springer, New York, USA, 2014
- [28] Oterkus, S., et al., Peridynamic Thermal Diffusion, *Journal Comput. Phys.*, 265 (2014), May, pp. 71-96
- [29] Gerstle, W., et al., *Peridynamic Simulation of Electromigration*, 8 (2008), 2, pp. 75-92
- [30] Bobaru, F., Duangpanya, M., A Peridynamic Formulation for Transient Heat Conduction in Bodies with Evolving Discontinuities, *Journal Comput. Phys.*, 231 (2012), 7, pp. 2764-2785
- [31] Jafari, A., Bahaaddini, R., Numerical Analysis of Peridynamic and Classical Models in Transient Heat Transfer, *Employing Galerkin Approach*, 47 (2017), 3, pp. 531-555
- [32] Chen, W., et al., A Refined Thermo-Mechanical Fully Coupled Peridynamics with Application Concrete Cracking, *Eng. Fract. Mech.*, 242 (2021), Feb., 107463
- [33] Agwai, A., A Peridynamic Approach for Coupled Fields, Ph. D. thesis, University of Arizona, Tucson, Ariz., USA, 2011
- [34] Liao, Y., et al., Peridynamic Simulation of Transient Heat Conduction Problems in Functionally Gradient Materials With Cracks, *UTHS*, 40 (2017), 12, pp. 1484-1501

- [35] Wang, L., *et al.*, A Peridynamic Framework and Simulation of Non-Fourier and Non-Local Heat Conduction, *Int. J. Heat Mass Transf.*, *118* (2018), Mar., pp. 1284-1292
- [36] Hosseini-Tehrani, P., Eslami, M. R., The BEM Analysis of Thermal and Mechanical Shock in A 2-D Finite Domain Considering Coupled Thermoelasticity, *Eng. Anal. Bound. Elem.*, *24* (2000), 3, pp. 249-257
- [37] Khalid, P., Thermoelastic Relaxation and Its Effects on the Compressibility of Pore Fluid and P Wave Velocities, *Arab. J. Geosci.*, *8* (2015), 8, pp. 6157-6167
- [38] Wu, S. C., *et al.*, Phase Leading of Temperature Variations in Cavity Caused by Heat Conduction between Air and Rock, *Chinese Phys. Lett.*, *20* (2003), 12, pp. 2192-2194
- [39] Zhang, Y., *et al.*, Peridynamic Simulation of Crack Propagation of Non-Homogeneous Brittle Rock-Like Materials, *Theor. Appl. Fract. Mech.*, *106* (2020), 102438
- [40] Zhou, L., *et al.*, Simulations of Fractures of Heterogeneous Orthotropic Fiber-Reinforced Concrete with Pre-Existing Flaws Using an Improved Peridynamic Model, *Materials (Basel)*, *15* (2022), 11, pp. 3977